Atomic multiwave interferometer for Aharonov-Casher-phase measurements

Min-Kang Zhou, Ke Zhang, Xiao-Chun Duan, Yi Ke, Cheng-Gang Shao, and Zhong-Kun Hu*

MOE Key Laboratory of Fundamental Physical Quantities Measurement, School of Physics, Huazhong University of Science and Technology, 1037 Luo Yu Road, Wuhan 430074, People's Republic of China

(Received 3 August 2015; published 24 February 2016)

We present an atomic multiwave interferometer with magnetic sublevels to precisely determine the Aharonov-Casher (AC) geometric phase. Simulations show that this interferometer has sharper fringes than a normal two-wave interferometer, which means a higher phase resolution can be achieved. Moreover, atoms evolving in a single hyperfine structure state make the interferometer insensitive to the dc Stark phase shift. This dc Stark shift is one of the main noise sources in AC phase measurements. The constraint of the photon rest mass is also discussed when using this atomic interferometer to measure the Aharonov-Casher phase.

DOI: 10.1103/PhysRevA.93.023641

I. INTRODUCTION

The Aharonov-Casher (AC) phase [1] is a typical geometric phase, which is induced by a potential without a classical force and is independent of the modulus velocity of the particle. If considering a neutral particle with a magnetic dipole moment μ, traveling along a closed path around a charged wire, then the particle should acquire an AC topological phase shift given by

$$\Delta\varphi_{\mathrm{AC}} = \frac{1}{\hbar c^2}\oint \mu \times \mathbf{E}\cdot d\mathbf{r}, \tag{1}$$

where $\mathbf{E}$ is the electric field due to the wire. The AC phase was directly observed [2] and measured [3–8] in some experiments. The first experiment that demonstrated the existence of the AC effect was done with a neutron interferometer with a precision of 24% [3]. To improve the sensitivity, atom interferometers based on Ramsey or Ramsey-Borde interferometry were made to measure the AC phase. People turned to the atom interferometer because the magnetic moment of some atoms is about 1000 times larger than that of a neutron, which can therefore increase the signal-to-noise ratio dramatically. The current best accuracy for AC phase measurements [5] has a relative uncertainty of 1.4%. It will be interesting to improve the precision by searching for new methods or sensors.

High-precision cold-atom interferometers could be the potential tools for accurate measurements of the AC phase. Cold-atom matter-wave interferometers were demonstrated to be valuable tools for precision inertial sensors [9–16], determining physical constants [17,18], and other fundamental research [19]. The Mach-Zehnder-type two-wave atom interferometers (AIs) have excited worldwide interests and are widely used in precision measurements. Atom interferometers composed of multiple matter waves, using either atomic momentum states or internal states, have also been proposed and demonstrated. Multiwave AIs with separated spatial paths were based on the momentum recoil scheme, realized by the optical pumping [20], the optical lattice [21–25], Raman laser pulses [26–28], or diffraction from optical standing waves [29–32]. Petrovic and co-workers [33,34] demonstrated a multiple-internal-state cold-atom interferometer with Zeeman sublevels in which the rf pulse combined with Raman transitions is used to couple different Zeeman states. Similar to the Fabry-Pérot optical interferometer, the multiwave AI has sharper fringe patterns, which leads to a higher phase resolution than the two-wave interferometer.

Inspired by Petrovic and co-workers, we present an atomic multiwave interferometer using only Raman laser pulses. Atoms are coupled to multiple magnetic Zeeman states by the first laser pulse through stimulated Raman transitions. Each Zeeman state represents an atomic matter wave. After a free evolution time T, these matter waves are recombined by another Raman pulse to form interference patterns. By selecting appropriate laser polarization and frequency, atoms stay in one angular momentum state, which makes this atom interferometer insensitive to the phase shift induced by the electric field. On the other hand, the atom interferometer is sensitive to the magnetic field because atoms are superposed in Zeeman states. This provides a promising way for magnetometry [35] and making other physical measurements related to the magnetic moment.

The magnetic moment of each arm in this multiwave interferometer is different. If we add a dc electric field on the atoms, according to Eq. (1), the accumulated Aharonov-Casher [5] phase is proportional to the difference of the magnetic quantum number Δm_F. Thus this multiwave AI with cold ^{87}Rb atoms can be employed to measure the AC phase. The dc Stark phase can be easily a dominant noise in AC phase measurements when high dc voltages are applied. However, in our scheme, interferences will happen between the magnetic sublevels of one hyperfine structure state ($|F=1\rangle$ or $|F=2\rangle$), so the main dc Stark phase shift due to scalar polarizability will vanish [7]. Considering the simplest case, we use a three-wave AI for theoretical analysis. The AC phase is expected to be measured with a relative resolution of 10^{-5} limited by the quantum projection noise.

II. MULTIWAVE ATOM INTERFEROMETER

We begin with the analysis of a three-wave AI by considering a five-level atom, which is denoted by $|a\rangle$, $|b\rangle$, $|c\rangle$, $|4\rangle$, and $|5\rangle$ in Fig. 1(a). The atom is illuminated by two copropagating linearly polarized laser beams (L1 and L2) with frequencies ω_{L1} and ω_{L2}, respectively. The polarization of one laser is along the quantum axes defined by the

*zkhu@mail.hust.edu.cn

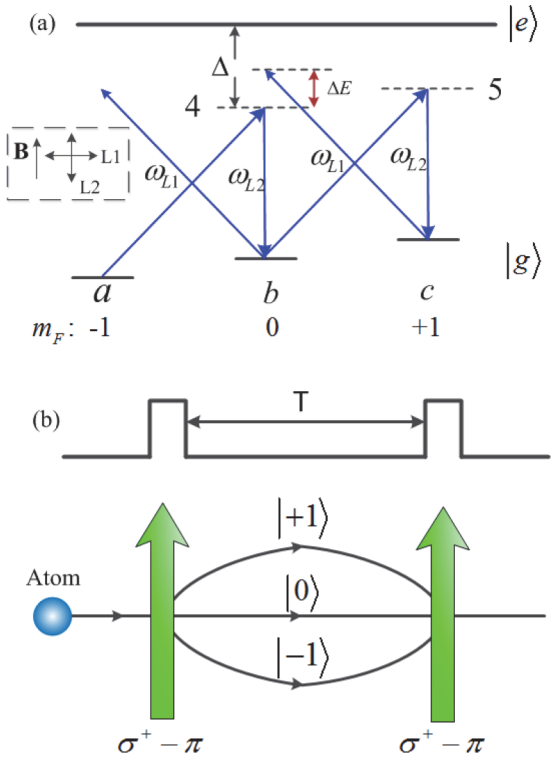

FIG. 1. (a) Level scheme for stimulated Raman transitions by two copropagating and perpendicular linearly polarized laser beams. The two beams have a large common frequency detuning Δ with respect to the atomic single-photon resonance. The inset shows the polarization of the Raman beams and the bias field. (b) Time sequence of a three-wave atom interferometer. The atom is illuminated by two Raman pulses with a time interval of T, which is similar to a Ramsey-type interferometer.

magnetic bias field B. The polarization of another laser is perpendicular to the quantum axes. Thus the two lin⊥lin lasers can be equivalent to the superposition of $\sigma^+ - \pi$ and $\sigma^- - \pi$ laser beams. As shown in Fig. 1(a), because of the resonance condition, either $\sigma^+ - \pi$ or $\sigma^- - \pi$ can drive the two-photon stimulated Raman transition between Zeeman states $|m_F\rangle$ and $|m_F + 1\rangle$. We will start the calculation of the interaction between five sublevels and Raman beams in the $\sigma^+(I_1) - \pi(I_2)$ configuration, where I_1 and I_2 are the intensities of two beams. The reason that we add the off-resonance beam $\sigma^-(I_1) - \pi(I_2)$ is because it can be used to compensate for the light shift, which will be explained later in this section.

The system Hamiltonian is given by

$$H = \sum_k \hbar\omega_k |k\rangle\langle k| - \mathbf{d}\cdot(\mathbf{E}_1 + \mathbf{E}_2), \quad k = (a,b,c,4,5), \quad (2)$$

where $\hbar\omega_k$ denotes the energy spacing between corresponding states, $\mathbf{d}$ is the atomic dipole moment, and $\mathbf{E}_{1\,(2)}$ represents the electric field of the σ^+ (π) laser. The laser field can be written as $\mathbf{E}_i = \mathbf{E}_{i0}\cos(\omega_i t + \varphi_i) = \mathbf{E}_{i0}(e^{i\omega_i t + i\varphi_i} + e^{-i\omega_i t - i\varphi_i})/2$. During the evolution, atoms are in a superposition state denoted by

$$|\psi\rangle = \sum_k c_k(t)|k\rangle e^{-i\omega_k t}, \quad k = (a,b,c,4,5), \quad (3)$$

where $c_k(t)$ is the time-dependent probability amplitude, which can be derived by solving the Schrödinger equation

$$\hat{H}|\psi\rangle = i\hbar\frac{\partial}{\partial t}|\psi\rangle. \quad (4)$$

Substituting Eqs. (2) and (3) into Eq. (4), the differential equations about $c_k(t)$ are given by

$$i\dot{c}_j = \sum_k c_k \Omega_{jk} e^{-i\omega_{kj}t}, \quad j = (a,b,c,4,5), \quad (5)$$

in which $\omega_{kj} = \omega_k - \omega_j$ is the frequency difference of two states. In this, the Rabi frequency $\Omega_{jk} = -\langle j|\mathbf{d}\cdot(\mathbf{E}_{10} + \mathbf{E}_{20})|k\rangle/\hbar$ represents the coupling strength. According to the selection rule, Ω_{a4} is nonzero only in the case of c_a. Thus, Eq. (5) becomes

$$\begin{aligned} i\dot{c}_a &= -c_4\langle a|\mathbf{d}\cdot(\mathbf{E}_{10} + \mathbf{E}_{20})|4\rangle e^{-i\omega_{4a}t}/\hbar \\ &= -c_4\langle a|\mathbf{d}\cdot(\mathbf{E}_{10}e^{i\omega_1 t - i\omega_{4a}t + i\phi_1} + \mathbf{E}_{10}e^{-i\omega_1 t - i\omega_{4a}t - i\phi_1} \\ &\quad + \mathbf{E}_{20}e^{i\omega_2 t - i\omega_{4a}t + i\phi_2} + \mathbf{E}_{20}e^{-i\omega_2 t - i\omega_{4a}t - i\phi_2})|4\rangle/2\hbar. \end{aligned} \quad (6)$$

The subsequent application of the rotating-wave approximation [36] allows us to consider only the slowly varying terms. In addition, because of polarization, laser 2 does not couple level $|a\rangle$ to $|4\rangle$. So Eq. (6) reduces to

$$\dot{c}_a = -ic_4\Omega_{1a4}e^{i\Delta_{14a}t + i\phi_1}/2, \quad (7)$$

in which $\Delta_{14a} = \omega_1 - \omega_{4a}$ is the frequency detuning of the laser field to the atomic resonance. Here the Rabi frequency is written as $\Omega_{1a4} = -\langle a|\mathbf{d}\cdot\mathbf{E}_{10}|4\rangle/\hbar$. We then find the rest of the coupled differential equations

$$\begin{aligned} \dot{c}_b &= -i(c_4\Omega_{2b4}e^{i\Delta_{24b}t + i\phi_2} + c_5\Omega_{1b5}e^{i\Delta_{15b}t + i\phi_1})/2, \\ \dot{c}_c &= -ic_5\Omega_{2c5}e^{i\Delta_{25c}t + i\phi_2}/2, \\ \dot{c}_4 &= -i(c_a\Omega_{14a}e^{-i\Delta_{14a}t - i\phi_1} + c_b\Omega_{24b}e^{-i\Delta_{24b}t - i\phi_2})/2, \\ \dot{c}_5 &= -i(c_b\Omega_{15b}e^{-i\Delta_{15b}t - i\phi_1} + c_c\Omega_{25c}e^{-i\Delta_{25c}t - i\phi_2})/2. \end{aligned} \quad (8)$$

Because the detuning Δ_{ljk} is larger than Ω_{ljk}, this system can be approximated by a three-level system with an effective electromagnetic field [36]. The intermediate states $|4\rangle$ and $|5\rangle$ are not populated, while Rabi oscillations can be driven between states $|a\rangle$ and $|b\rangle$, as well as $|b\rangle$ and $|c\rangle$. Thus the evolution equations of the three-level system are

$$\begin{aligned} \dot{c}_a &= -\frac{i\Omega_{1a4}^2}{4\Delta}c_a - \frac{i\Omega_{1a4}\Omega_{2b4}}{4\Delta}e^{i\delta t + i\phi_{12}}c_b, \\ \dot{c}_b &= -\frac{i\Omega_{1a4}\Omega_{2b4}}{4\Delta}e^{-i\delta t - i\phi_{12}}c_a - \frac{i\Omega_{1b5}^2 + i\Omega_{2b4}^2}{4\Delta}c_b \\ &\quad - \frac{i\Omega_{1b5}\Omega_{2c5}}{4\Delta}e^{i\delta t + i\phi_{12}}c_c, \\ \dot{c}_c &= -\frac{i\Omega_{1b5}\Omega_{2c5}}{4\Delta}e^{-i\delta t - i\phi_{12}}c_b - \frac{i\Omega_{2c5}^2}{4\Delta}c_c, \end{aligned} \quad (9)$$

where $\Delta_{14a} = \Delta_{24b} = \Delta_{15b} = \Delta_{25c} = \Delta$, $\delta = \omega_{12} + \omega_{ba} = \omega_{12} + \omega_{cb}$, and $\phi_{12} = \phi_1 - \phi_2$. The differential equations of motion for the interaction wave function $|\psi(t)\rangle = \{c_a, c_b, c_c\}^T$

are determined by the Hamiltonian shown in

$$V_{\rm s}=\begin{pmatrix} -i\delta_{{\rm AC}a} & -\frac{i\Omega_{1a4}\Omega_{2b4}}{4\Delta}e^{i\delta t+i\phi_{12}} & 0 \\ -\frac{i\Omega_{1a4}\Omega_{2b4}}{4\Delta}e^{-i\delta t-i\phi_{12}} & -i\delta_{{\rm AC}b} & -\frac{i\Omega_{1b5}\Omega_{2c5}}{4\Delta}e^{i\delta t+i\phi_{12}} \\ 0 & -\frac{i\Omega_{1b5}\Omega_{2c5}}{4\Delta}e^{-i\delta t-i\phi_{12}} & -i\delta_{{\rm AC}c} \end{pmatrix}, \tag{10}$$

where $\delta_{{\rm AC}i}$ represents the ac Stark shift of each state induced by the light fields. So Eqs. (9) can be written as

$$\frac{\partial|\psi(t)\rangle}{\partial t}=V_{\rm s}|\psi(t)\rangle. \tag{11}$$

The time dependence in Eq. (10) can be eliminated by transferring into a rotating frame, turning with the detuning δ, and the new wave function becomes $|\psi(t)\rangle_{\rm R}=D|\psi(t)\rangle$, so Eq. (11) can be written as

$$\frac{\partial|\psi(t)\rangle_{\rm R}}{\partial t}=\left(DV_{\rm s}D^{\dagger}-D\frac{\partial D^{\dagger}}{\partial t}\right)|\psi(t)\rangle_{\rm R}=H_{\rm R}|\psi(t)\rangle_{\rm R}, \tag{12}$$

where the transformation matrix is

$$D=\begin{pmatrix} e^{-i\delta t/\,2} & & \\ & e^{+i\delta t/\,2} & \\ & & e^{+3i\delta t/\,2} \end{pmatrix}.$$

This manipulation leads to the stationary Hamiltonian

$$H_{\rm R}=\begin{pmatrix} -i(\delta+2\delta_{{\rm AC}a})/2 & -i\Omega_{\rm eff}e^{i\phi} & 0 \\ -i\Omega_{\rm eff}e^{-i\phi} & i(\delta-2\delta_{{\rm AC}b})/2 & -i\Omega_{\rm eff}e^{i\phi} \\ 0 & -i\Omega_{\rm eff}e^{-i\phi} & i(3\delta-2\delta_{{\rm AC}c})/2 \end{pmatrix}, \tag{13}$$

where $\phi=\phi_{12}$ and $\Omega_{\rm eff}=\frac{\Omega_{1a4}\Omega_{2b4}}{4\Delta}=\frac{\Omega_{1b5}\Omega_{2c5}}{4\Delta}$ denotes the effective Rabi frequency. If we take an example that the ground state is in $|5^2S_{1/2},F=1\rangle$ of the ^{87}Rb D_2 line, the ground state ($|a\rangle$, $|b\rangle$, or $|c\rangle$) corresponds to the magnetic substate ($|m_F=-1\rangle$, $|m_F=0\rangle$, or $|m_F=+1\rangle$), and after employing the transition matrix elements, the ac Stark shift of each state becomes

$$\begin{aligned}
\delta_{{\rm AC}a}&=\alpha I_1\left(\frac{1/\,6}{\Delta}+\frac{5/\,24}{\Delta+0.072}+\frac{1/\,24}{\Delta+0.072+0.157}\right)+\alpha I_2\left(\frac{5/\,24}{\Delta+0.072}+\frac{1/\,8}{\Delta+0.072+0.157}\right),\\
\delta_{{\rm AC}b}&=\alpha I_1\left(\frac{5/\,24}{\Delta+0.072}+\frac{1/\,8}{\Delta+0.072+0.157}\right)+\alpha I_2\left(\frac{1/\,6}{\Delta}+\frac{1/\,6}{\Delta+0.072+0.157}\right),\\
\delta_{{\rm AC}c}&=\alpha I_1\left(\frac{1/\,4}{\Delta+0.072+0.157}\right)+\alpha I_2\left(\frac{5/\,24}{\Delta+0.072}+\frac{1/\,8}{\Delta+0.072+0.157}\right),
\end{aligned} \tag{14}$$

in which $\alpha=d^2/\hbar^2\varepsilon_0 c$. The big detuning Δ is normally 10 GHz and the intensities of the σ^+ and π lasers are $I_1=I_2=100$ mW/cm^2. The light shift for each state is obviously unequal. For example, the difference between states $|-1\rangle$ and $|0\rangle$ is $\delta_{{\rm AC}b}-\delta_{{\rm AC}a}\approx-18.6$ Hz. Then the accumulated phase shift is $2\pi(\delta_{{\rm AC}b}-\delta_{{\rm AC}a})\tau\approx2.3\times10^{-3}$ rad during the second π pulse of 20 μs. It should be considered when the AI is used for precision measurement. However, when we take into account the off-resonance σ^- light of laser 1 that is put aside, the light shifts become

$$\begin{aligned}
\delta_{{\rm AC}a}&=\alpha I_1\left(\frac{1/\,6}{\Delta}+\frac{5/\,24}{\Delta+0.072}+\frac{1/\,24}{\Delta+0.072+0.157}+\frac{1/\,4}{\Delta+0.072+0.157}\right)+\alpha I_2\left(\frac{5/\,24}{\Delta+0.072}+\frac{1/\,8}{\Delta+0.072+0.157}\right),\\
\delta_{{\rm AC}b}&=\alpha I_1\left(\frac{5/\,24}{\Delta+0.072}+\frac{1/\,8}{\Delta+0.072+0.157}+\frac{5/\,24}{\Delta+0.072}+\frac{1/\,8}{\Delta+0.072+0.157}\right)+\alpha I_2\left(\frac{1/\,6}{\Delta}+\frac{1/\,6}{\Delta+0.072+0.157}\right),\\
\delta_{{\rm AC}c}&=\alpha I_1\left(\frac{1/\,4}{\Delta+0.072+0.157}+\frac{1/\,24}{\Delta}+\frac{5/\,24}{\Delta+0.072}+\frac{1/\,6}{\Delta+0.072+0.157}\right)+\alpha I_2\left(\frac{5/\,24}{\Delta+0.072}+\frac{1/\,8}{\Delta+0.072+0.157}\right).
\end{aligned} \tag{15}$$

Now the difference of light shifts is (in Hz)

$$\begin{aligned}
\delta_{{\rm AC}b}-\delta_{{\rm AC}a}&=\alpha I_1\left(-\frac{1/\,6}{\Delta}+\frac{5/\,24}{\Delta+0.072}-\frac{1/\,24}{\Delta+0.072+0.157}\right)+\alpha I_2\left(\frac{1/\,6}{\Delta}-\frac{5/\,24}{\Delta+0.072}+\frac{1/\,24}{\Delta+0.072+0.157}\right)\\
&=-1.2I_1+1.2I_2.
\end{aligned} \tag{16}$$

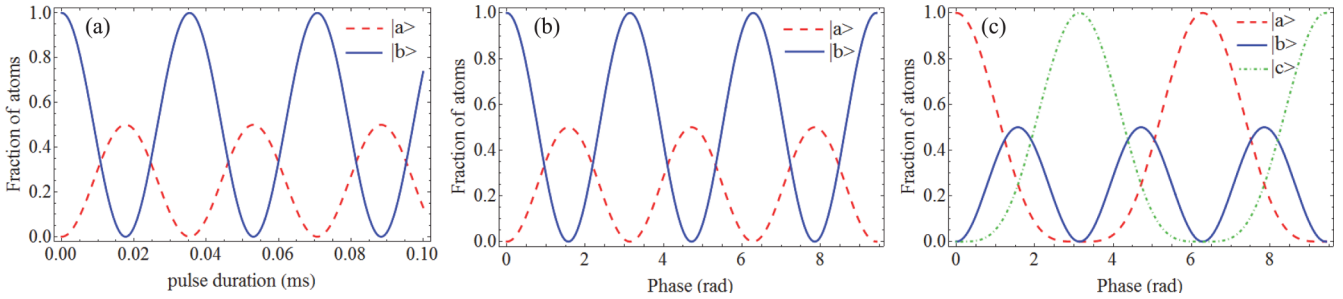

FIG. 2. (a) Three-wave Rabi oscillation. (b) Interference fringes when atoms are prepared in initial state $|b\rangle$. (c) Interference fringes in initial state $|c\rangle$. In all the graphs, the solid line represents the possibility of atoms in state $|b\rangle$. The red and green dashed lines represent state $|a\rangle$ and state $|c\rangle$, respectively.

When I_1 and I_2 are comparable within 1%, the difference of light shifts can decrease to 10^{-5} rad after taking into account the laser polarization fluctuation, which is two orders smaller than the case of only σ^+ light. Thus we can say that this type of AI is insensitive to the light shift, which is all denoted by δ_{AC}.

After solving Eq. (12), we are able to obtain the phase behavior after t once we know the initial wave function. It can be written as

$$|\psi(t)\rangle = U(\Omega_{\mathrm{eff}},t,\delta,\delta_{\mathrm{eff}})|\psi(0)\rangle, \tag{17}$$

where U is the evolution matrix of ground states, which is shown in Eq. (18) for zero detuning $\delta = 0$. Here we define $\omega = \sqrt{\delta^2 + 2\Omega_{\mathrm{eff}}^2}$ for simplicity:

$$U = \frac{e^{-it\delta_{\mathrm{AC}}}}{2}\begin{pmatrix} 1+\cos(\omega t) & -i\sqrt{2}\sin(\omega t)e^{i\phi} & [\cos(\omega t)-1]e^{2i\phi} \\ -i\sqrt{2}\sin(\omega t)e^{-i\phi} & 2\cos(\omega t) & -i\sqrt{2}\sin(\omega t)e^{i\phi} \\ [\cos(\omega t)-1]e^{-2i\phi} & -i\sqrt{2}\sin(\omega t)e^{-i\phi} & 1+\cos(\omega t) \end{pmatrix}. \tag{18}$$

Assuming an initial wave function of this three-state system $|\psi(0)\rangle = \{0,1,0\}^T$, the transition probabilities of the three states as a function of pulse length τ are $P_a(\tau) = P_c(\tau) = \sin^2(\sqrt{2}\Omega_{\mathrm{eff}}\tau)/2$ and $P_b(\tau) = \cos^2(\sqrt{2}\Omega_{\mathrm{eff}}\tau)$, respectively. The Rabi oscillation obtained by numerical simulation is shown in Fig. 2(a), while the Rabi frequency is set to $2\pi \times 10^4$ Hz. As we can see, all the population flows from state $|b\rangle$ to states $|a\rangle$ and $|c\rangle$ with the same probability with pulse time $\tau = \frac{\pi}{2\sqrt{2}\Omega_{\mathrm{eff}}} = 17.7\ \mu$s. So this type of Raman pulse is similar to the so-called π pulse in a two-level system; when $\tau = 8.8\ \mu$s, it is the $\pi/2$ pulse.

We can form the three-wave interferometer with a sequence of two Raman pulses. When atoms are in an initial state of $m_F = 0$, the first Raman pulse splits them into the superposition of state $m_F = 0$ and state $m_F = \pm 1$. After a free evolution time T, the second pulse recombines the three matter waves, which then interfere with each other. We can get the interference patterns using

$$|\psi(t)\rangle = U_2(\tau)U_1(\tau)|\psi(0)\rangle. \tag{19}$$

Similar to the mirrors used in a Fabry-Pérot interferometer, we employ two π pulses to form the multiwave atom interferometer. The transition probabilities of three states $m_F = -1,0,+1$ after two π pulses are found are

$$P_a = P_c = \tfrac{1}{2}\sin^2(\varphi_2 - \varphi_1), \quad P_b = \cos^2(\varphi_2 - \varphi_1), \tag{20}$$

which are shown in Fig. 2(b) as a function of the phase difference of two Raman pulses. If we now assume that all atoms are initially prepared in state $m_F = +1$, the relative

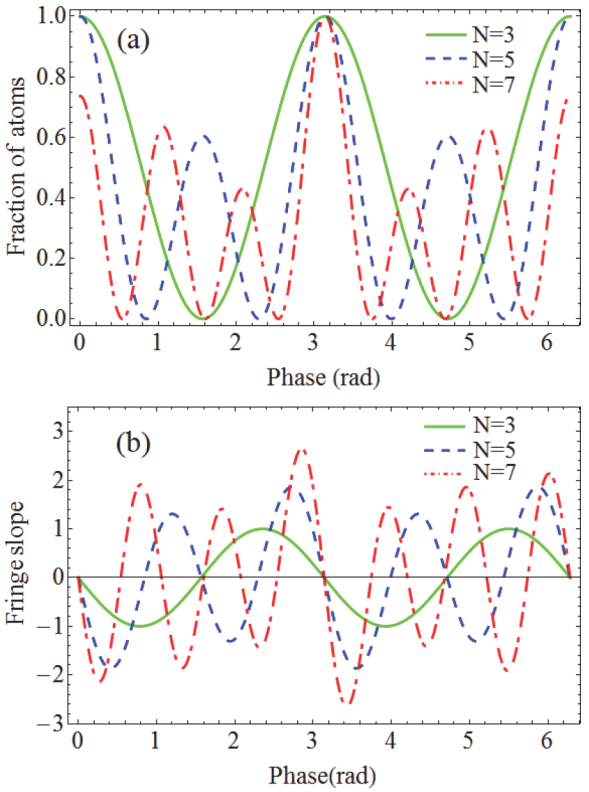

FIG. 3. (a) Calculated interference patterns of Ramsey atomic multiwave interferometer with three, five, and seven waves. (b) Comparison of the midfringe slope in three cases of AI.

populations of three states after two π pulses are

$$\begin{aligned} P_a &= \cos^4[(\varphi_2-\varphi_1)/2], \\ P_b &= \tfrac{1}{2}\sin^2(\varphi_2-\varphi_1), \\ P_c &= \sin^4[(\varphi_2-\varphi_1)/2], \end{aligned} \tag{21}$$

which are shown in Fig. 2(c).

To increase the sensitivity, atom interferometers are usually locked at two neighboring points at midfringe [37], which has a maximal slope $dP/d\varphi$. In the measurement, from the difference between two consecutive measured transition probabilities, the phase error can be evaluated and then used to correct φ_2. Using this method, we can increase the sampling rate and reject common mode noises due to the Raman laser or the instability of the system. The maximum slope reaches 1 rad^{-1} in Fig. 2(b) of state $|b\rangle$ and the maximum decreases to 0.65 rad^{-1} in Fig. 2(c) of state $|a\rangle$ or $|c\rangle$. Obviously, we choose to prepare the atoms initially in state $m_F = 0$ to get higher resolution. Compared to 0.5 rad^{-1} of the typical two-wave AI, this three-wave AI reaches a double-fringe resolution. The imperfect polarization of Raman beams can cause the pulse distortion, which may make the fringe unstable and cause phase noise and thus will increase the measurement uncertainty. However, we notice that the laser pulse duration is only tens of microseconds and the extinction ratio of the laser polarization can easily reach 10^3:1 with a Glan-laser polarizer, thus the phase resolution could be as good as 10^{-6} rad with an integration time of 10^4 s.

Then there is particular interest in increasing the number of matter waves in this type of atom interferometer. It is necessary to choose atoms whose ground state $|g\rangle$ is composed of multiple Zeeman sublevels. Based on this, we can form an equivalent N-level system with the same configuration of Raman beams. In this N-wave AI, the duration of the π pulse is still the half period of the Rabi oscillation. According to the calculated evolution matrix, the interference pattern is obtained by using Eq. (19) with an initial state $|m_F = 0\rangle$. Figure 3 shows the simulated fringes and their differential with a different number N of matter waves ($N = 3,5,7$). As N increases, the fringe becomes sharper and its maximum slope is bigger. The seven-wave atom interferometer achieves a slope of 2.65 rad^{-1}, which means that it has 5.3 times higher resolution than that of the two-wave interferometer. Even though the fringe shape becomes more complicated, we can use the fringe-locking method to overcome it, which means the AI just works on two adjacent points of the largest slope of the fringe.

For a large number of waves where $N > 7$, assuming a zero-frequency detuning, the stationary Hamiltonian matrix is written as Eq. (22). The interference pattern is obtained using eigenvalue analysis to solve the differential equations

$$H_R = \begin{pmatrix} 0 & -i\Omega_{\text{eff}}e^{i\phi} & & & \cdots & \\ -i\Omega_{\text{eff}}e^{-i\phi} & 0 & -i\Omega_{\text{eff}}e^{i\phi} & & & \\ & \cdots & \cdots & \cdots & & \\ & & -i\Omega_{\text{eff}}e^{-i\phi} & 0 & -i\Omega_{\text{eff}}e^{i\phi} & \\ \cdots & & \cdots & -i\Omega_{\text{eff}}e^{-i\phi} & 0 & -i\Omega_{\text{eff}}e^{i\phi} \\ & & & & -i\Omega_{\text{eff}}e^{-i\phi} & 0 \end{pmatrix}. \tag{22}$$

III. MEASUREMENT SCHEME FOR THE AHARONOV-CASHER EFFECT

Because atoms are usually the ideal test mass for precision measurements, we use them here to detect the Aharonov-Casher phase. In this scheme, we choose the three-wave interferometer of cold ^{87}Rb atoms for the simulation and the experimental schematic is shown in Fig. 4.

The ^{87}Rb atoms are loaded into a two-dimensional (2D) magneto-optical trap (MOT). During the loading, a repumping light guarantees that all atoms are in the $|5^2S_{1/2}, F = 2\rangle$ state. The initial mean velocity of the cooled atoms is about 50 m/s in the x direction when atoms free fall from a typical 2D MOT. Then a bias magnetic field in the $-y$ direction is used to define the quantization axis and all the atoms are optically pumped into the $|F = 1, m_F = 0\rangle$ state by a single selective Raman π pulse. The remaining atoms are blown away by a resonant light pulse from $|F = 2\rangle$ to $|F' = 3\rangle$.

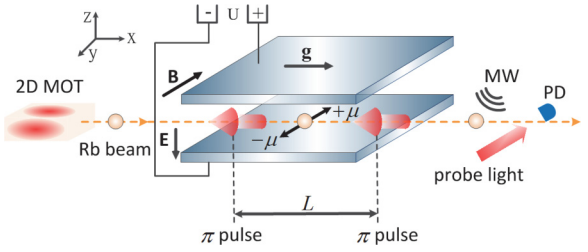

FIG. 4. Experimental schematic for measurements of the Aharonov-Casher phase: MW, microwave; PD, photodiode.

The zone where the actual interference measurement is taking place is located in a capacitor with a magnetic shield. The capacitor is composed of a pair of stainless steel plates that are 1.05 m long, 10 mm wide, and spaced by 10 mm. We apply a large homogeneous electric field of $E = 1$ MV/m in the $-z$ direction for an applied voltage $V = 10$ kV. The three-wave interferometer is realized by the atoms interacting with a sequence of $\sigma^+ - \pi$ Raman pulses with the duration of 17.7 μs. The Raman pulses are composed of two copropagating linearly polarized Raman laser beams that are red tuned about 10 GHz below the $F = 1 \rightarrow F' = 0$ resonance of the D_2 line and they propagate against the atoms, which are separated by a distance $L = 1$ m.

During the free evolution, two wave packets of $m_F = -1$ and $m_F = +1$ states with opposite magnetic dipole moment go through the electric field on the same path and experience the AC phase shift. To get the interference signal, a microwave pulse is applied to select atoms in the $m_F = 0$ state for

detecting. The obtained interference pattern can be calculated based on the former section. Adding the free evolution operator

$$U_{\mathrm{T}} = \begin{pmatrix} e^{-i\phi_{\mathrm{f}}} & 0 & 0 \\ 0 & 1 & 0 \\ 0 & 0 & e^{i\phi_{\mathrm{f}}} \end{pmatrix},$$

Eq. (19) becomes

$$|\psi(t)\rangle = U_{\pi} U_{\mathrm{T}} U_{\pi} |\psi(0)\rangle, \tag{23}$$

where φ_{f} is the phase shift due to free evolution of the atoms between the electrode. Then the probability of atoms in the $m_F = 0$ state is given by

$$P_0 = \cos^2(\Delta\varphi + \varphi_{\mathrm{f}}) = [1 - \cos 2(\Delta\varphi + \varphi_{\mathrm{f}})]/2, \tag{24}$$

where $\Delta\varphi$ is the phase difference of two Raman pulses. Here $\varphi_{\mathrm{f}} = \varphi_{\mathrm{AC}} + \varphi_{\mathrm{Z}}$ includes the AC phase and the Zeeman phase shift due to the residual magnetic field. The huge dc Stark effect has been canceled out during the interference because all the atoms are in the same hyperfine structure state. However, considering the high-order Stark shift [38–40], there is a frequency shift between states $|\pm 1\rangle$ and $|0\rangle$ that is written as

$$\Delta\nu_{10} = \Delta\nu(5S_{1/2}, 1, \pm 1) - \Delta\nu(5S_{1/2}, 1, 0) = -\tfrac{1}{4}\alpha_2^{(3)} E^2. \tag{25}$$

Here $-\alpha_2^{(3)}/4 = -104.4 \times 10^{-10}$ Hz/(V/cm)^2 is the third-order tensor polarizability [39] and E is the applied dc electric field. After some calculation, the accumulated phase shift is $\varphi_{\mathrm{dS}} \approx 0.3$ rad, which is comparable to the AC phase. According to $\alpha_2^{(3)}$, atoms in states $|m_F = \pm 1\rangle$ have the same dc Stark shift $f_{+1\mathrm{dc}} = f_{-1\mathrm{dc}} \approx 1$ Hz with respect to state $|m_F = 0\rangle$. During the free evolution stage after the first π pulse, atoms are only in a superposition of states $|m_F = +1\rangle$ and $|m_F = -1\rangle$, thus the interference phase shift φ_{dc} due to the dc Stark effect is zero, because $\varphi_{\mathrm{dc}} = (f_{-1\mathrm{dc}} - f_{+1\mathrm{dc}})T = 0$. Therefore, this atom interferometer is insensitive to the dc Stark effect. The dc Stark phase shift will also appear during the laser pulse duration. Because the pulse lasts several microseconds, this phase shift is about 10^{-5} rad, which can be neglected.

The Zeeman phase shift will dominate the systematic errors during the AC phase measurements. Since the Zeeman effect is independent of the electric field and the AC phase shift is relative to the direction of the applied electric field according to Eq. (1), we infer that we can change the direction of the electric field and make a differential measurement to extract only the AC phase. The theoretical interference fringe as shown in Fig. 2(b) is obtained by sweeping the phase of the second Raman pulse. The phase shift between different voltage configurations can be thought of as the AC phase $\varphi_{\mathrm{AC}} = \frac{1}{2}[\varphi_{\mathrm{f}}(+V) - \varphi_{\mathrm{f}}(-V)]$.

The resulting AC phase between states $|+1\rangle$ and $|0\rangle$ is about 0.5 rad calculated by theoretical expression $\varphi_{\mathrm{AC}} = -\frac{\mu E L}{\hbar c^2}$. The phase resolution of this multiwave AI will be limited by the quantum projection noise, which depends on the number of atoms. The atomic loading rate of a 2D MOT is usually at a level of 10^{10} atoms/s. If we set the single measurement time for 1s, according to the loading rate, after the state selection and thermal diffusion, about 10^8 atoms are supposed to contribute to the interferometer signal. From Eq. (24), the phase noise of this AI is $\delta\varphi = 1/2C\sqrt{N}$ due to shot noise, where C is the fringe contrast and N is the number of detected atoms. Then the AC phase resolution becomes $\delta\varphi/\varphi_{\mathrm{AC}} = 1/C\sqrt{N}$; it is supposed to be 10^{-5} at an integration time of 100 s, after averaging the phase combination of two configurations. In addition, if we choose suitable atoms such as some isotopes of heavy atoms to form an N-wave AI that contains more interfering matter waves, the higher phase resolution can be obtained due to the sharper fringes. We also expect that the accuracy will improve by comparing the former experiments, after we estimate the system effects induced by electromagnetic field. In a real experiment, some other effects such as the electric fringe field between the capacitor should be considered carefully to reach a relative uncertainty of 10^{-5}.

We can bound the rest mass m_γ of the photon through the measurement of the AC phase [41]; there will be a deviation from the AC phase through the modification of electrostatic field. The effect of a nonzero photon rest mass can be incorporated into electromagnetism straightforwardly through the Proca equations [42,43]. In the Proca version, the potential between the capacitor is given by

$$\Phi(z) = \left(\frac{e^{-\mu_\gamma (d-z)}}{2\mu_\gamma} - \frac{e^{-\mu_\gamma z}}{2\mu_\gamma} \right) \frac{\sigma}{\varepsilon_0}, \tag{26}$$

where $\mu_\gamma^{-1} = \hbar/m_\gamma c$ is the Compton wavelength of the photon, d is the electrode spacing, σ is the surface charge density, and the position of plate with negative charge is $z = 0$. Then the electric field is

$$\begin{aligned} E(z) &= -\nabla\Phi(z) = -\frac{\sigma}{\varepsilon_0} \left(\frac{e^{-\mu_\gamma (d-z)} + e^{-\mu_\gamma z}}{2} \right) \\ &= E_0 \left(\frac{e^{-\mu_\gamma (d-z)} + e^{-\mu_\gamma z}}{2} \right). \end{aligned} \tag{27}$$

Using a first-order approximation, this becomes $E(z) = E_0(1 - \mu_\gamma d/2)$; $E(z)$ approaches $E_0 = -\sigma/\varepsilon_0$ as μ_γ vanishes, which is the standard electric field of the electrode. In comparison, if $\delta E/E = \delta\varphi/\varphi_{\mathrm{AC}} = 10^{-5}$, we would get $\mu_\gamma = 2 \times 10^{-3}$ m^{-1} and the detectable photon rest mass is 7×10^{-43} g according to Eq. (27). If we apply a voltage of 100 kV and increase the atom number to 10^{10}, the expected limit on m_γ is 7×10^{-47} g with an integration time of 12 days, which is comparable to other experiments [44] for bounding the rest mass of the photon. Observing the AC phase in different spacing d of the capacitor but keeping the same electric field will be helpful in determining the photon rest mass. By comparing the ratio $\varphi_{\mathrm{AC1}}/\varphi_{\mathrm{AC2}} = (2 - \mu_\gamma d_1)/(2 - \mu_\gamma d_2)$ of each of two measurements, we can get the Compton wavelength μ_γ directly without knowing the absolute value of the electric field.

IV. CONCLUSION

We have presented a method for measuring the Aharonov-Casher phase by an atomic multiwave interferometer, which employs the multiple ground-state Zeeman sublevels driven by stimulated Raman transitions. This multiwave AI is insensitive to both the dc and ac Stark phase shifts. The Zeeman shift

can be canceled out by applying an opposite electric field. Moreover, sharper fringes will be obtained by using a large number of atomic waves, which means that a higher phase sensitivity can be reached compared to the normal two-wave interferometer. According to the simulations, the measurable AC phase accumulated in the multiwave interferometer can be larger than 0.5 rad and a relative resolution of 10^{-5} in an integration time of 100 s is expected. The constraint on the rest mass of photon is also discussed by considering the deviation from the AC phase.

ACKNOWLEDGMENTS

This work was supported by the National Natural Science Foundation of China (Grants No. 11474115, No. 11205064, and No. 11204094).

[1] Y. Aharonov and A. Casher, Phys. Rev. Lett. **53**, 319 (1984).
[2] M. König, A. Tschetschetkin, E. M. Hankiewicz, J. Sinova, V. Hock, V. Daumer, M. Schäfer, C. R. Becker, H. Buhmann, and L. W. Molenkamp, Phys. Rev. Lett. **96**, 076804 (2006).
[3] A. Cimmino, G. I. Opat, A. G. Klein, H. Kaiser, S. A. Werner, M. Arif, and R. Clothier, Phys. Rev. Lett. **63**, 380 (1989).
[4] K. Sangster, E. A. Hinds, S. M. Barnett, E. Riis, and A. G. Sinclair, Phys. Rev. A **51**, 1776 (1995).
[5] A. Görlitz, B. Schuh, and A. Weis, Phys. Rev. A **51**, R4305 (1995).
[6] K. Zeiske, G. Zinner, F. Riehle, and J. Helmcke, Appl. Phys. B **60**, 205 (1995).
[7] S. Yanagimachi, M. Kajiro, M. Machiya, and A. Morinaga, Phys. Rev. A **65**, 042104 (2002).
[8] J. Gillot, S. Lepoutre, A. Gauguet, J. Vigué, and M. Büchner, Eur. Phys. J. D **68**, 168 (2014).
[9] A. Peters, K. Y. Chung, and S. Chu, Metrologia **38**, 25 (2001).
[10] T. Farah, C. Guerlin, A. Landragin, P. Bouyer, S. Gaffet, F. Pereira Dos Santos, and S. Merlet, Gyroscopy Navigation **5**, 266 (2014).
[11] Z. K. Hu, B. L. Sun, X. C. Duan, M. K. Zhou, L. L. Chen, S. Zhan, Q. Z. Zhang, and J. Luo, Phys. Rev. A **88**, 043610 (2013).
[12] M. Hauth, C. Freier, V. Schkolnik, A. Senger, M. Schmidt, and A. Peters, Appl. Phys. B **113**, 49 (2013).
[13] J. M. McGuirk, G. T. Foster, J. B. Fixler, M. J. Snadden, and M. A. Kasevich, Phys. Rev. A **65**, 033608 (2002).
[14] T. L. Gustavson, A. Landragin, and M. A. Kasevich, Class. Quantum Grav. **17**, 2385 (2000).
[15] M. K. Zhou, Z. K. Hu, X. C. Duan, B. L. Sun, L. L. Chen, Q. Z. Zhang, and J. Luo, Phys. Rev. A **86**, 043630 (2012).
[16] M. K. Zhou, X. C. Duan, L. L. Chen, Q. Luo, Y. Y. Xu, and Z. K. Hu, Chin. Phys. B **24**, 050401 (2015).
[17] A. Wicht, J. Hensley, E. Sarajlic, and S. Chu, Phys. Scr. **T102**, 82 (2002).
[18] G. Rosi, F. Sorrentino, L. Cacciapuoti, M. Prevedelli, and G. M. Tino, Nature (London) **510**, 518 (2014).
[19] D. Schlippert, J. Hartwig, H. Albers, L. L. Richardson, C. Schubert, A. Roura, W. P. Schleich, W. Ertmer, and E. M. Rasel, Phys. Rev. Lett. **112**, 203002 (2014).
[20] M. Weitz, T. Heupel, and T. W. Hänsch, Phys. Rev. Lett. **77**, 2356 (1996).
[21] B. P. Anderson and M. A. Kasevich, Science **282**, 1686 (1998).
[22] S. Fray, C. A. Diez, T. W. Hänsch, and M. Weitz, Phys. Rev. Lett. **93**, 240404 (2004).
[23] M. Fattori, C. D'Errico, G. Roati, M. Zaccanti, M. Jona-Lasinio, M. Modugno, M. Inguscio, and G. Modugno, Phys. Rev. Lett. **100**, 080405 (2008).
[24] M. Gustavsson, E. Haller, M. J. Mark, J. G. Danzl, R. Hart, A. J. Daley, and H. C. Nägerl, New J. Phys. **12**, 065029 (2010).
[25] M. K. Zhou, B. Pelle, A. Hilico, and F. Pereira dos Santos, Phys. Rev. A **88**, 013604 (2013).
[26] H. Hinderthür, F. Ruschewitz, H. J. Lohe, S. Lechte, K. Sengstock, and W. Ertmer, Phys. Rev. A **59**, 2216 (1999).
[27] F. Impens and C. J. Bordé, Phys. Rev. A **80**, 031602 (2009).
[28] T. Aoki, K. Shinohara, and A. Morinaga, Phys. Rev. A **63**, 063611 (2001).
[29] K. J. Hughes, J. H. T. Burke, and C. A. Sackett, Phys. Rev. Lett. **102**, 150403 (2009).
[30] M. R. de Saint Vincent, J. P. Brantut, C. J. Bordé, A. Aspect, T. Bourdel, and P. Bouyer, Europhys. Lett. **89**, 10002 (2010).
[31] B. Barrett, I. Chan, and A. Kumarakrishnan, Phys. Rev. A **84**, 063623 (2011).
[32] W. D. Li, T. C. He, and A. Smerzi, Phys. Rev. Lett. **113**, 023003 (2014).
[33] J. Petrovic, I. Herrera, P. Lombardi, F. Schaefer, and F. S. Cataliotti, New J. Phys. **15**, 043002 (2013).
[34] P. Lombardi, F. Schaefer, I. Herrera, S. Cherukattil, J. Petrovic, C. Lovecchio, F. Marin, and F. S. Cataliotti, Opt. Express **22**, 19141 (2014).
[35] M. K. Zhou, Z. K. Hu, X. C. Duan, B. L. Sun, J. B. Zhao, and J. Luo, Phys. Rev. A **82**, 061602 (2010).
[36] P. R. Berman, *Atom Interferometry* (Academic, New York, 1997).
[37] X. C. Duan, M. K. Zhou, D. K. Mao, H. B. Yao, X. B. Deng, J. Luo, and Z. K. Hu, Phys. Rev. A **90**, 023617 (2014).
[38] P. G. H. Sandars, Proc. Phys. Soc. **92**, 857 (1967).
[39] H. Gould, E. Lipworth, and M. C. Weisskopf, Phys. Rev. **188**, 24 (1969).
[40] S. Ulzega, A. Hofer, P. Moroshkin, and A. Weis, Europhys. Lett. **76**, 1074 (2006).
[41] C. Fuchs, Phys. Rev. D **42**, 2940 (1990).
[42] A. Proca, J. Phys. Radium Ser. VII **7**, 347 (1936).
[43] A. Proca, J. Phys. Radium Ser. VII **8**, 23 (1937).
[44] L. C. Tu, J. Luo, and G. T. Gillies, Rep. Prog. Phys. **68**, 77 (2005).